IEEE Robotics and Automation Letters (RAL) paper presented at the
2020 IEEE/RSJ International Conference on Intelligent Robots and Systems (IROS)
October 25-29, 2020, Las Vegas, NV, USA (Virtual)

Energy-Efficient Locomotion Generation and Theoretical Analysis of a Quasi-passive Dynamic Walker

Longchuan Li[1], *Isao Tokuda[2] and Fumihiko Asano[3]

***Abstract*— This paper presents a robot walking control method, which we call "quasi-passive dynamic walking." The method is targeted at underactuated legged robots and applied to obtain energy-efficient limit cycle gait on level ground. To achieve efficient locomotion, as well as to overcome the underactuation of the system, two key points are implemented into this method to positively utilize the passive dynamics of the system. The first one is to initialize the walker at the fixed Poincaré section obtained from passive dynamic walking on a gentle downhill. The second one is to indirectly excite the hip angle by periodically oscillating a wobbling mass, which is attached to the body frame. The walker is, therefore, able to step forward on level ground without any torque actuation. Moreover, the phase diagram of the generated gait is entrained to limit cycle by the periodical oscillation of the wobbling mass. Numerical simulations and theoretical analysis are conducted to evaluate the efficiency as well as the local stability of the gait. Our control method enables underactuated legged robots to walk extremely efficiently on level ground with only one actuator, which provides the easiness for implementation on real machines.**

I. INTRODUCTION

Legs enable humans and most of the mammals to flexibly select the contacting points for locomotion, which provides their capability of traveling to the furthest distance. The methods for controlling gait of contemporary legged robots are, therefore, designed to be extraordinarily versatile so that they can not only traverse many different terrains, but also perform a sequence of dynamic maneuvers that form a gymnastic routine [1]–[4].

On the other hand, high energy efficiency of these locomotion robots is inevitable for applying them to real tasks in human daily life. In contrast to the versatile control paradigms which generate special tricks, another kind of walking prototype that walks at a single cadence, namely limit cycle walking [5], [6], is more practical in common locomotion. This locomotion is inspired by passive dynamic walking on the downhill [7]–[9], which walks without any input and achieves a stable periodical gait through a dexterity design of their configurations and the gravity only. Similar periodical gait can be generated on the level ground through limit cycle walking with, however, low efficiency. Some studies improved the efficiency of limit cycle walking by tracking the trajectories of mechanical energy restoration [10]–[12] and achieved successful results. However, it is difficult to implement their control methods in real conditions, due to the requirement of full actuation.

In order to enable underactuated [13] legged robots to walk efficiently and stably on level ground, this paper comes up with a novel control method, which we call "quasi-passive dynamic walking (QPDW)" by positively utilizing the passive dynamics of the system. As illustrated in Fig. 1, the quadruped locomotion robot is composed of two identical and symmetric compass-like biped walkers, which are connected by a body frame. The hip joints are passive, *i.e.*, no actuator is applied. Alternatively, an active wobbling mass, which can be controlled to oscillate in parallel with the body frame, is attached to it. We define the direction of "X" in Fig. 1 as the front. Angles of the right foreleg and the left hind leg (in blue color) are synchronized with each other by mechanical constraints and so is the other side (in red color). Such a configuration reduces the rotation momentum during the legs swing motion [14], as well as reduces the required degrees of freedom to model the system.

To design a locomotion paradigm that positively utilizes the passive dynamics of the system, the QPDW gait is initialized at the fixed Poincaré section obtained from passive dynamic walking on a gentle downhill (PDWGD), inspired by the phenomenon observed from the ideal condition of passive dynamic walking on the level ground (PDWLG). In addition, the wobbling mass is forced to oscillate periodically to indirectly excite the hip angle, as well as to entrain the

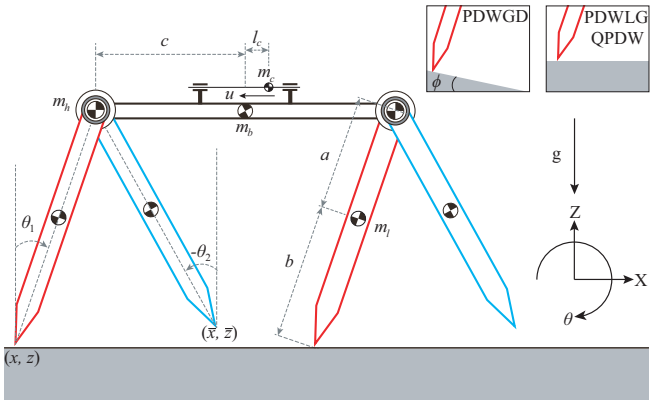

Fig. 1. Mathematical model of quasi-passive dynamic walker

This work was supported by the Japan Society for the Promotion of Science under Grant-in-aid for Science Research (No. 17H06313, No. 20K11875). *(Corresponding author: Isao Tokuda.)*

[1]Longchuan Li is with the Research Organization of Science and Technology, Ritsumeikan University, 1-1-1 Nojihigashi, Kusatsu, Shiga 525-8577, Japan (e-mail: lltt2144@fc.ritsumei.ac.jp).

[2]Isao Tokuda is with the Department of Mechanical Engineering, Ritsumeikan University, 1-1-1 Nojihigashi, Kusatsu, Shiga 525-8577, Japan (e-mail: isao@fc.ritsumei.ac.jp).

[3]Fumihiko Asano is with the School of Information Science, Japan Advanced Institute of Science and Technology, 1-1 Asahidai, Nomi, Ishikawa 923-1292, Japan (e-mail: fasano@jaist.ac.jp).

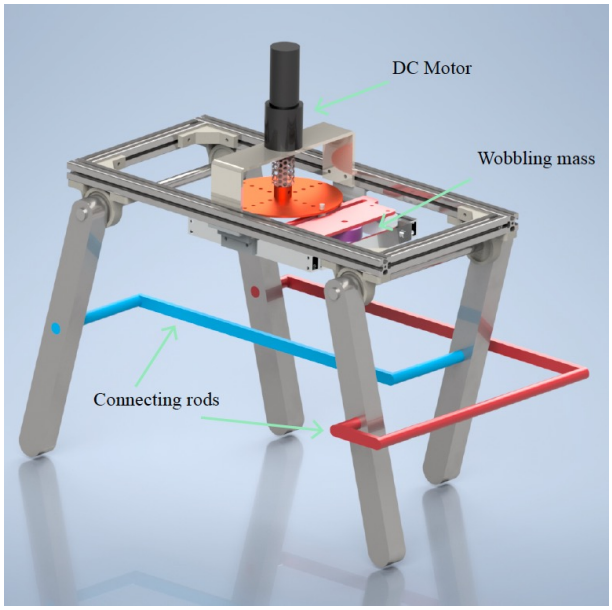

Fig. 2. Machine design of quasi-passive dynamic walker

gait to limit cycle. Extremely energy-efficient gait can be achieved by our control method, and its local stability is proven via the return map.

II. PASSIVE DYNAMIC WALKING

This section introduces the passive dynamics of this walker, as a prior knowledge for the following sections.

A. Equation of Motion

As illustrated in Fig. 1, the position of grounding point on the hind side is (x,z) [m], the angular positions of the support and swing legs to the vertical are θ_1 [rad] and θ_2 [rad], respectively. Besides, the displacement of the wobbling mass with respect to the center is l_c [m]. In addition, the body frame is always in parallel with the ground, due to the identicality, symmetry and synchrony between the fore and hind legs. Fig. 2 shows the detailed mechanisms of the legs synchronization realized by the connecting rods, and the mass wobbling motion realized by mapping it to the rotation of a DC motor via piston crank linkage. The generalized coordinate of the system is: $\boldsymbol{q} = \begin{bmatrix} x & z & \theta_1 & \theta_2 & l_c \end{bmatrix}^{\mathrm{T}}$. The walker is placed on a gentle slope with the angular position of ϕ [rad], and its swing legs generate a pendulum-like motion autonomously according to the following equation:

$$\boldsymbol{M}\ddot{\boldsymbol{q}} + \boldsymbol{h} = \boldsymbol{J}^{\mathrm{T}}\boldsymbol{\lambda}. \tag{1}$$

Here, $\boldsymbol{M}$ is the inertia matrix, $\boldsymbol{h}$ is the combination of centrifugal force, Coriolis force and gravity terms. The details are shown as follows:

$$\boldsymbol{M} = \begin{bmatrix} m_t & 0 & (lm_t - 2am_l)C_1 & -2am_lC_2 & m_cC_\phi \\ & m_t & -(lm_t - 2am_l)S_1 & 2am_lS_2 & -m_cS_\phi \\ & & 2(l^2+b^2)m_l + l^2m_s & -2alm_lC_{\Delta_{12}} & lm_cC_{\Delta_{\phi 1}} \\ & & & 2a^2m_l & 0 \\ \text{Sym.} & & & & m_c \end{bmatrix},$$

$$\boldsymbol{h} = \begin{bmatrix} -\dot{\theta}_1^{\,2}(lm_t - 2am_l)S_1 + 2a\dot{\theta}_2^{\,2}m_lS_2 \\ m_tg - \dot{\theta}_1^{\,2}(lm_t - 2am_l)C_1 + 2a\dot{\theta}_2^{\,2}m_lC_2 \\ -g(lm_t - 2am_l)S_1 - 2a\dot{\theta}_2^{\,2}lm_lS_{\Delta_{12}} \\ 2am_l(\dot{\theta}_1^{\,2}lS_{\Delta_{12}} + gS_2) \\ -gm_cS_\phi + \dot{\theta}_1^{\,2}lm_cS_{\Delta_{\phi 1}} \end{bmatrix},$$

where

$$\begin{aligned} m_t &= m_b + m_c + 2m_h + 4m_l, \quad m_s = m_b + m_c + 2m_h, \\ l &= a + b, \quad S_\angle = \sin\angle, \quad C_\angle = \cos\angle, \quad \angle = \theta_1, \theta_2, \phi \\ C_{\Delta_{12}} &= \cos(\theta_1 - \theta_2), \quad S_{\Delta_{12}} = \sin(\theta_1 - \theta_2), \\ C_{\Delta_{\phi 1}} &= \cos(\phi - \theta_1), \quad S_{\Delta_{\phi 1}} = \sin(\phi - \theta_1). \end{aligned}$$

Besides, $\boldsymbol{J}$ is the Jacobian matrix for holonomic constraints and $\boldsymbol{\lambda}$ is the constraint forces vector. The grounding point is assumed to be fixed, *i.e.*, $\dot{x} = 0$ and $\dot{z} = 0$. In addition, the wobbling mass is mechanically locked at the center of the body under the condition of passive dynamic walking, which results in $\dot{l}_c = 0$. By summarizing these constraints, the detailed constraint equation $\boldsymbol{J}$ is shown as follows:

$$\begin{bmatrix} 1 & 0 & 0 & 0 & 0 \\ 0 & 1 & 0 & 0 & 0 \\ 0 & 0 & 0 & 0 & 1 \end{bmatrix} \dot{\boldsymbol{q}} = \boldsymbol{J}\dot{\boldsymbol{q}} = \boldsymbol{0}_{3\times 1}. \tag{2}$$

Thus, the dynamics of the legs swing motion can be derived by solving Eq. (1) with the time derivative of Eq. (2) at the same time.

B. Collision Equation

According to the symmetry of the legs configuration, the zero-crossing of the following function:

$$f(\theta_1, \theta_2) := \theta_1 + \theta_2 - 2\phi, \tag{3}$$

from negative, which requires $\frac{\mathrm{d}}{\mathrm{d}t}f(\theta_1,\theta_2) := \dot{\theta}_1 + \dot{\theta}_2 > 0$, is used for detecting the collision. Simultaneously, the support and swing legs exchange according to inelastic collision model:

$$\boldsymbol{M}\dot{\boldsymbol{q}}^+ = \boldsymbol{M}\dot{\boldsymbol{q}}^- + \boldsymbol{J}_I^{\mathrm{T}}\boldsymbol{\lambda}_I, \tag{4}$$

where the superscripts $+$ and $-$ represent the instant immediately after and before the collision, respectively, and $\boldsymbol{J}_I$ and $\boldsymbol{\lambda}_I$ represent the constraint matrix and constraint forces vector at landing instant. Define the position of foot tip of the hind swing leg as $(\bar{x},\bar{z})$ [m] as shown in Fig. 1. Besides, assume $\dot{\bar{x}} = 0$, $\dot{\bar{z}} = 0$ and $\dot{l}_c = 0$ at the collision instant. The constraint equation at landing instant is therefore summarized as:

$$\begin{bmatrix} 1 & 0 & l\cos\theta_1 & -l\cos\theta_2 & 0 \\ 0 & 1 & -l\sin\theta_1 & l\sin\theta_2 & 0 \\ 0 & 0 & 0 & 0 & 1 \end{bmatrix} \dot{\boldsymbol{q}}^+ = \boldsymbol{J}_I\dot{\boldsymbol{q}}^+ = \boldsymbol{0}_{3\times 1}. \tag{5}$$

Note that the parameter c [m], which indicates half length of the body frame as shown in Fig. 1, is neither involved in the swing motion nor ground collision, since the fore and hind legs are always assumed to be synchronized with each other.

C. Return Map

The existence of steady state phase in passive dynamic walking has been already well investigated in the literature, and its local stability, *i.e.*, the existence of limit cycle, is usually addressed by the following discrete return map (or Poincaré map) [8]:

$$\boldsymbol{Q}_{k+1} = \boldsymbol{P}(\boldsymbol{Q}_k), \tag{6}$$

where $\boldsymbol{Q}_k$ is the state vector at the beginning of k^{th} step, since the Poincaré section of the return map for legged locomotion is normally defined as the instant immediately after ground collision. Besides, $\boldsymbol{P}$ is the return map of the state vector $\boldsymbol{Q}$ from the current step k to the next step $k+1$, and the selection of the state vector will be discussed later.

In steady locomotion, the state maps to itself neglect the step number:

$$\boldsymbol{Q}^* = \boldsymbol{P}(\boldsymbol{Q}^*). \tag{7}$$

Once a slight disturbance is applied to the i^{th} dimension of steady state, the output of the return map becomes:

$$\boldsymbol{Q}^* + \boldsymbol{\delta}_1^i = \boldsymbol{P}(\boldsymbol{Q}^* + \boldsymbol{\delta}_0^i) \approx \boldsymbol{P}(\boldsymbol{Q}^*) + \left.\frac{\partial \boldsymbol{P}}{\partial \boldsymbol{Q}}\right|_{\boldsymbol{Q}^*} \boldsymbol{\delta}_0^i, \tag{8}$$

where the perturbation on the i^{th} dimension of steady state is represented by vector $\boldsymbol{\delta}_0^i$, and its resultant deviation is defined as $\boldsymbol{\delta}_1^i$. Therefore, the gradient matrix can be derived by substituting Eq. (7) into Eq. (8) after applying perturbation to each dimension respectively:

$$\left.\frac{\partial \boldsymbol{P}}{\partial \boldsymbol{Q}}\right|_{\boldsymbol{Q}^*} \approx \begin{bmatrix} \boldsymbol{\delta}_1^1 & \boldsymbol{\delta}_1^2 & \cdots & \boldsymbol{\delta}_1^n \end{bmatrix} \begin{bmatrix} \boldsymbol{\delta}_0^1 & \boldsymbol{\delta}_0^2 & \cdots & \boldsymbol{\delta}_0^n \end{bmatrix}^{-1}. \tag{9}$$

Defining the i^{th} eigenvalue of matrix $\left.\frac{\partial \boldsymbol{P}}{\partial \boldsymbol{Q}}\right|_{\boldsymbol{Q}^*}$ as λ_i, the gait is locally stable if $\max|\lambda_i| < 1$.

III. PROBLEM DESCRIPTION

This section numerically compares two kinds of gait patterns: steady state PDWGD and the ideal condition of PDWLG.

The gait of PDWGD is initialized at a suitable state on a gentle slope with the physical parameters listed in Tab. I. The hip angle $\alpha = \theta_1 - \theta_2$ is plotted as the red curve in Fig. 3 (a), where the transient is removed, *i.e.*, only steady state of α is plotted. The ideal dynamics of PDWLG is initialized at the fixed Poincaré section obtained from PDWGD, while changing the slope angle ϕ to 0. The hip angle α of PDWLG is plotted as the dashed green curve. The PDWGD gait shows a periodical pattern, while the PDWLG gait decays gradually. The mechanism behind the periodical locomotion associated with PDWGD is the restoration of mechanical energy. Namely, the kinetic energy consumed by ground collision is supplied by gravitational potential energy. Without such an energy supply, PDWLG is unable to generate a similar gait. On the other hand, one can observe that the walking frequency f_w of PDWLG increases gradually, as shown in Fig. 3 (b). Note that, although it may look like converging to the walking frequency of PDWGD, this does not indicate a steady state behavior. The walking will eventually stop if no external actuation is applied. Fig. 4 shows the phase-plane portrait and the variation of the Poincaré section. The two trajectories start from the same phase. The trajectory of PDWGD generates a limit cycle, whose Poincaré section returns to itself in steady state phase. The trajectory of PDWLG, on the other hand, varies. These results together indicate that under the condition of initializing the gait of PDWLG at a suitable state, the kinetic energy could raise the walker's center of mass (CoM) until its potential energy reaches the highest point in one walking cycle, so that the walker can step forward by inversely transforming potential energy into kinetic energy. This process is also called overcoming the potential barrier [15]. The walker is, however, unable to go far away, since its hip angle shows damped oscillations. This simulation result is consistent with [16].

TABLE I
PARAMETERS OF CONFIGURATION.

m_l	1	kg
m_h	5	kg
m_c	1	kg
a	0.5	m
b	0.5	m
ϕ	0.01	rad
g	9.81	m/s^2

IV. QUASI-PASSIVE DYNAMIC WALKING

Inspired by the phenomenon of "damped oscillation rather than fall down" observed from PDWLG, this section introduces a QPDW control method that indirectly excites the hip

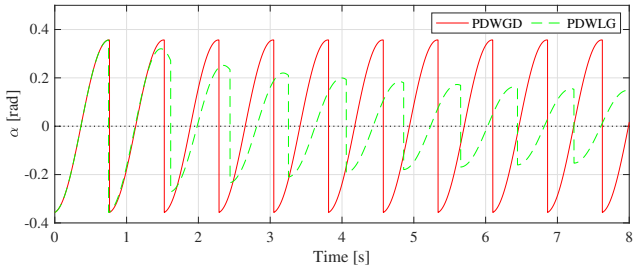

(a) Hip angle

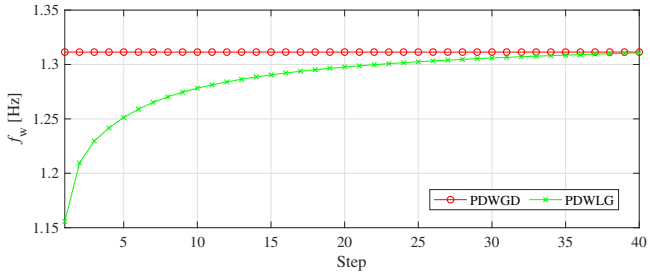

(b) Walking frequency

Fig. 3. Gait simulation of passive dynamic walking

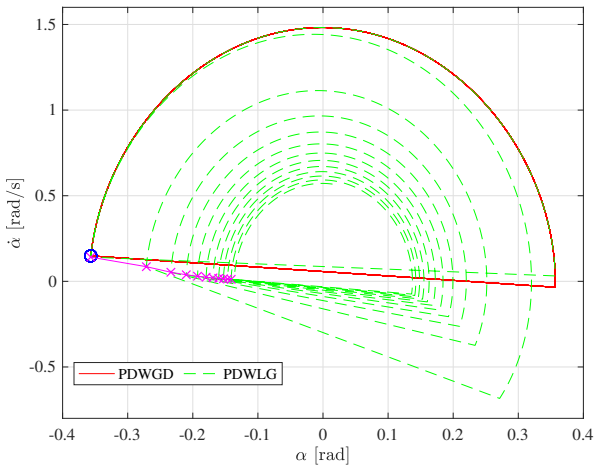

Fig. 4. Phase-plane portrait and Poincaré section (the instants that immediately after feet landing) of passive dynamic walking.

angle efficiently by positively utilizing the passive dynamics.

Our previous works have already shown that the walking frequency of the legged robots can be entrained to a periodically moved wobbling mass [17], [18], and the rotation amplitude of the sliding robots can be similarly controlled by this mechanism [19] [20]. We, therefore, introduce a wobbling mass to the walker to excite the amplitude of hip angle, as well as to entrain the walking frequency of the gait.

To enable the wobbling motion, the last rows of $\boldsymbol{J}$ and $\boldsymbol{J}_I$ in Eqs. (2) and (5) should be removed. Consequently, the equation of motion can be obtained by revising Eq. (1) to:

$$\boldsymbol{M}\ddot{\boldsymbol{q}} + \boldsymbol{h} = \boldsymbol{J}^{\mathrm{T}}\boldsymbol{\lambda} + \boldsymbol{S}u, \tag{10}$$

where u is the control input and $\boldsymbol{S} = \begin{bmatrix} 0 & 0 & 0 & 0 & 1 \end{bmatrix}^{\mathrm{T}}$ is the driving vector that specifies the actuation on the wobbling mass. Note that the actuation of the wobbling mass is model-free under the condition of applying the method on a real machine [17], since it is independent of the state and the parameters of the walker. However, for conducting the numerical simulation, it is better to use a model-based method that accurately tracks the trajectory of the wobbling mass.

The displacement of the wobbling mass l_c can be expressed as: $l_c = \boldsymbol{S}^{\mathrm{T}}\boldsymbol{q}$, and its 2nd order derivative with respect to time becomes:

$$\ddot{l_c} = \boldsymbol{S}^{\mathrm{T}}\ddot{\boldsymbol{q}}. \tag{11}$$

In addition, $\ddot{\boldsymbol{q}}$ can be derived from the equation of motion

TABLE II
PARAMETERS OF CONTROLLER.

A_m	0.05	m
f_c	1.26	Hz
K_{D}	40	s^{-2}
K_{P}	400	s^{-1}

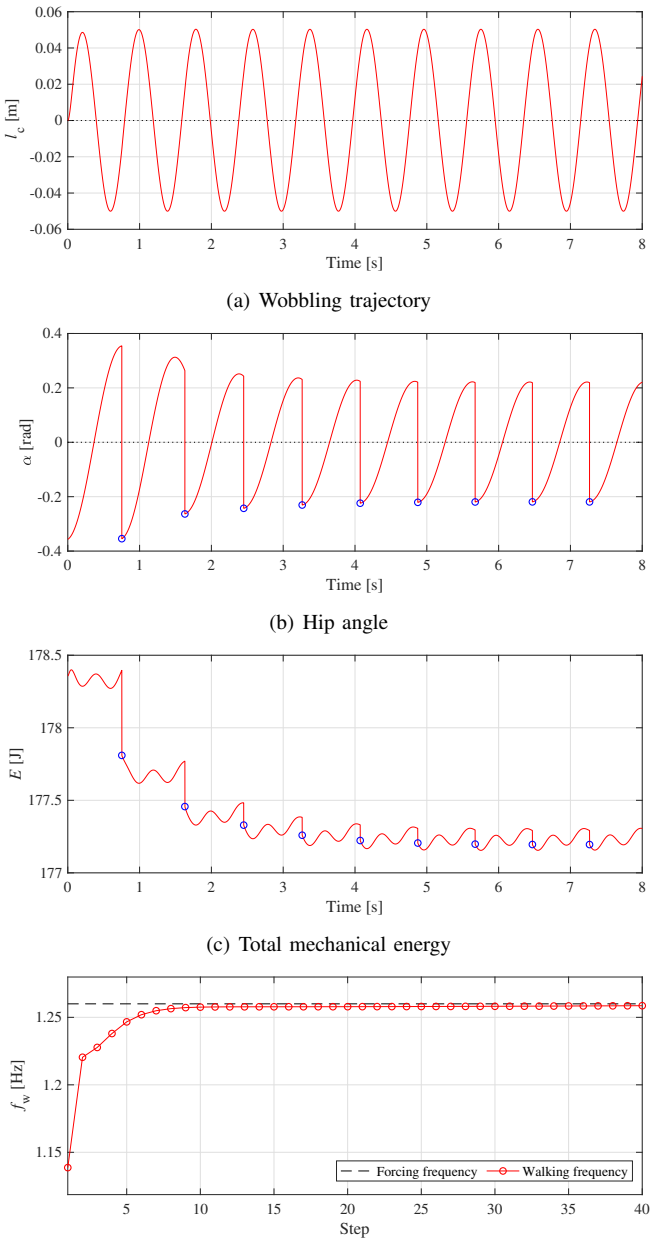

(a) Wobbling trajectory

(b) Hip angle

(c) Total mechanical energy

(d) Walking frequency

Fig. 5. Gait simulation of quasi-passive dynamic walking

and constraints:

$$\ddot{\boldsymbol{q}} = \boldsymbol{M}^{-1}\boldsymbol{Y}(\boldsymbol{S}u - \boldsymbol{h}), \tag{12}$$

where $\boldsymbol{Y} := \boldsymbol{I}_5 - \boldsymbol{J}^{\mathrm{T}}\boldsymbol{X}^{-1}\boldsymbol{J}\boldsymbol{M}^{-1}$, $\boldsymbol{X} := \boldsymbol{J}\boldsymbol{M}^{-1}\boldsymbol{J}^{\mathrm{T}}$, and $\boldsymbol{I}_5$ is an identity matrix of order 5. By substituting Eq. (12) into Eq. (11), the relationship between input and output becomes:

$$\ddot{l_c} = \boldsymbol{S}^{\mathrm{T}}\boldsymbol{M}^{-1}\boldsymbol{Y}(\boldsymbol{S}u - \boldsymbol{h}) = Au - B, \tag{13}$$

where $A := \boldsymbol{S}^{\mathrm{T}}\boldsymbol{M}^{-1}\boldsymbol{Y}\boldsymbol{S}$ and $B := \boldsymbol{S}^{\mathrm{T}}\boldsymbol{M}^{-1}\boldsymbol{Y}\boldsymbol{h}$. The input u that enables the wobbling mass to track a desired waveform $l_d(t)$ can be obtained by a PD controller:

$$\begin{aligned} u &= A^{-1}(v + B), \\ v &= \ddot{l}_d(t) + K_{\mathrm{D}}(\dot{l}_d(t) - \dot{l}_c) + K_{\mathrm{P}}(l_d(t) - l_c), \end{aligned} \tag{14}$$

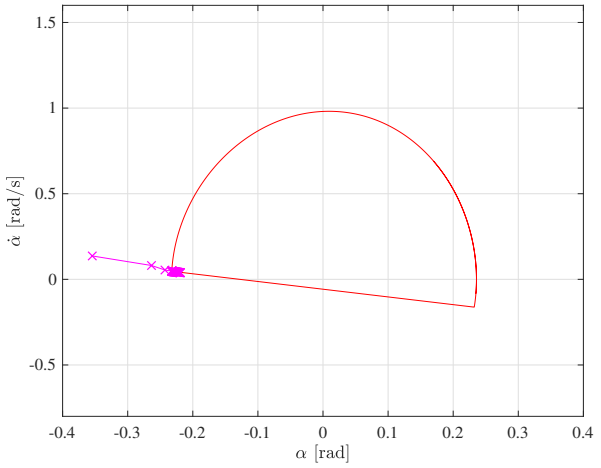

Fig. 6. Phase-plane portrait and Poincaré section (the instants that immediately after feet landing) of quasi-passive dynamic walking.

where K_{D} [s^{-1}] and K_{P} [s^{-2}] are the PD control gains. To smoothly affect the dynamics of the walker, the desired periodical trajectory for the wobbling mass is set to a sine waveform:

$$l_d(t) = A_m \sin(2\pi f_c t), \tag{15}$$

where A_m [m], f_c [Hz] are the desired amplitude and frequency for the wobbling motion, respectively.

To easily entrain the gait, the frequency of wobbling motion should be close to the natural frequency of the walking, which can be estimated from Fig. 3 (b). Parameters in Tab. I and II are used for the simulation of QPDW, except $\phi = 0$. The results are shown in Fig. 5. The trajectory of the wobbling mass accurately follows the desired sine waveform via the tracking control method, as shown in Fig. 5 (a). Moreover, Fig. 5 (b) shows that the periodical oscillation of the wobbling mass excites the amplitude of the hip angle effectively. The damped oscillation of the hip angle is avoided after a short transient. The blue circles indicate the instants immediately after the feet landing, which leads to the consumption of kinetic energy, as shown in Fig. 5 (c). Despite the energy loss, kinetic energy of the walker can be supplied by the wobbling motion in the condition of QPDW. In addition, Fig. 5 (d) shows that the walking frequency converges gradually to the wobbling frequency, indicating the occurrence of the entrainment. Benefited from this phenomenon, the dynamics converges to a limit cycle. Moreover, variation of the Poincaré section and the steady state phase-plane portrait are shown in Fig. 6, where the transient is removed for a clear demonstration of the limit cycle.

V. MOTION ANALYSIS

This section systematically conducts theoretical motion analysis on speed, efficiency and local stability of the QPDW.

A. Speed and Efficiency

Four gait descriptors are used to evaluate the walking performance: walking frequency f_w, hip angle at impact instant α_I, walking speed V_x and specific resistance SR. The walking speed is the product of walking frequency and stride, which is determined by the leg length l and the impact hip angle α_I:

$$V_x := f_w \times 2l \sin\frac{\alpha_I}{2}. \tag{16}$$

The specific resistance (also called cost of transport) is given by the ratio between the input energy and the mechanical work the walker did:

$$SR := \frac{p}{m_t g |V_x|}, \tag{17}$$
$$p := f_w \int_{200}^{200+\frac{1}{f_w}} |\dot{l}_c u| \mathrm{d}t.$$

The first 200 [s] of the locomotion, which is considered as the transient, is eliminated.

The gait descriptors are calculated using the parameter values listed in Tab. I and II, except that $\phi = 0$ and the wobbling frequency f_c is varied from 1.2 [Hz] to 1.31 [Hz]. The wobbling frequency is set close to natural walking frequency of the PDWGD, which is estimated to be around 1.31 [Hz] from Fig. 3 (b). The increment is set to 0.002 [Hz], where 20 steps of gait descriptors are calculated for each wobbling frequency. The walking frequency is shown in Fig. 7. The gait is entrained to the wobbling motion until $f_c = 1.296$ [Hz], and after that they are desynchronized with each other. Note that the plotted intervals are unequal, meaning that no value are calculated at some points. This is because the basin of attraction of the limit cycle is so small that suitable initial conditions are difficult to be found. Besides, Fig. 8 shows the impact hip angle α_I, where one can observe a jump at $f_c = 1.26$ [Hz], after which the hip angle is effectively excited. In addition, Fig. 9 indicates that the walking speed is mainly affected by α_I, rather than f_w. Moreover, the QPDW gait is extremely efficient, as shown in Fig. 10.

B. Phase Difference

Since the generated gaits demonstrate significantly different performances on the speed before and after $f_c = 1.26$ [Hz], here we analyze the nonlinear dynamics via the phase difference between the walker and the wobbling mass to explain this phenomenon. The phase difference ψ is defined as follows:

$$\psi := \frac{2\pi(t_l - t_p)}{T_w}, \tag{18}$$

where T_w represents the duration of walking in one cycle as shown in Fig. 11. t_l denotes the instant when the wobbling motion reaches half cycle, *i.e.*, the middle of sine waveform. In addition, t_p denotes the instant when the support legs are perpendicular to the ground, which is further approximated as the timing of overcoming the potential barrier, since θ_1 and θ_2 cross 0 almost simultaneously.

Note that t_p corresponds to the phase, at which the walker has the lowest kinetic energy, and t_l corresponds to the phase of the wobbling mass at the equilibrium point. One can expect that the phase difference ψ corresponds to the kinetic energy K_{cw} injected into the walker by the wobbling motion via the following relationship:

$$K_{cw} \propto |\sin \psi|, \tag{19}$$

since the wobbling trajectory forms a sine waveform.

In a similar manner as the last subsection, we calculate the phase difference ψ with respect to the wobbling frequency. The results are plotted in Fig. 12. By comparing the results with Fig. 8 and 9, one can observe that small values of α_I and low speed walking correspond to in-phase synchronization between the walker and the wobbling mass, *i.e.*, $\psi \approx 0$. Noteworthy are large values of α_I and high speed walking that appear around $\psi = -\pi/2$. These results are consistent with Eq. 19.

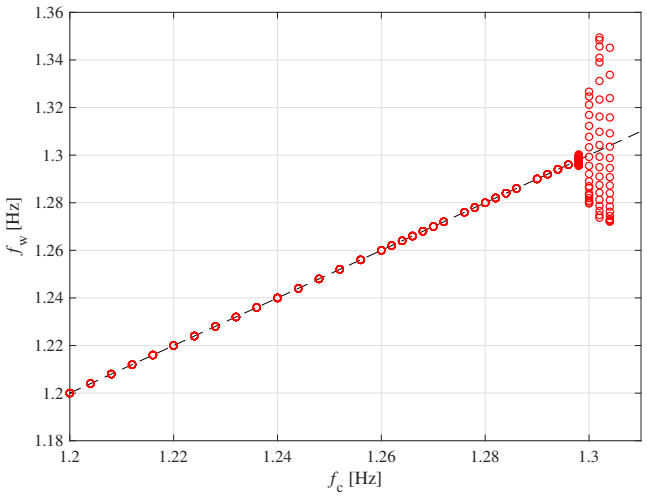

Fig. 7. Walking frequency versus wobbling frequency

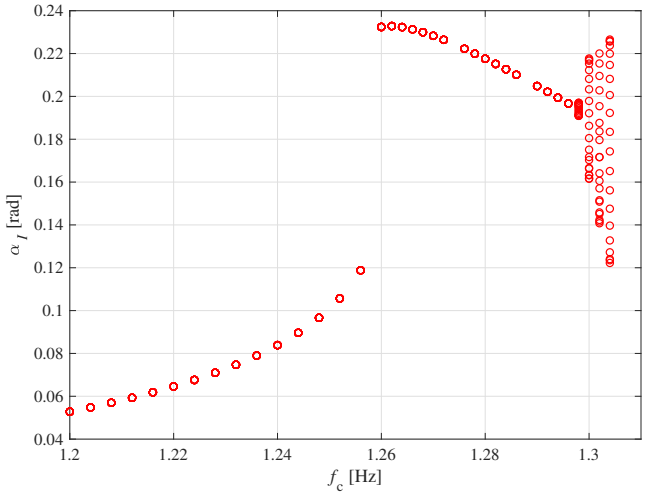

Fig. 8. Impact hip angle versus wobbling frequency

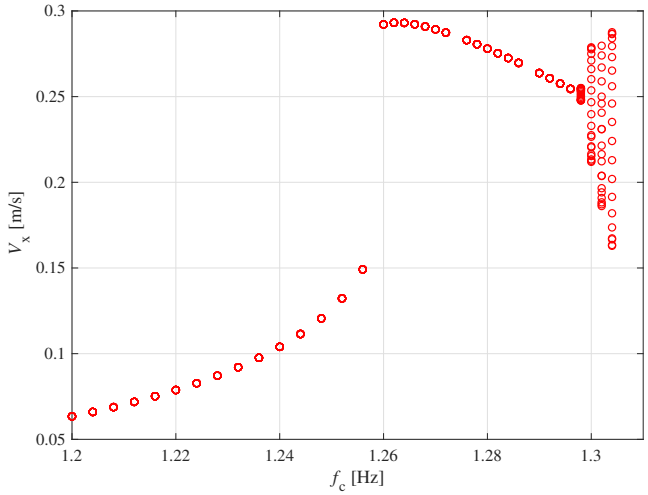

Fig. 9. Walking speed versus wobbling frequency

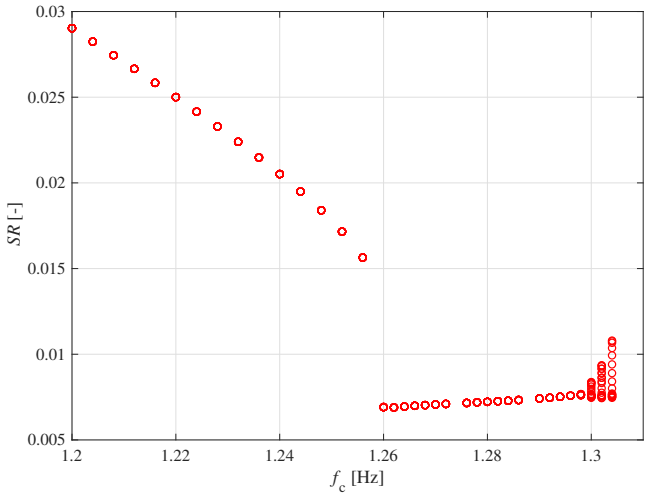

Fig. 10. Specific resistance versus wobbling frequency

C. *Local stability*

Although we mentioned in V-A that the basin of attraction of some gaits are so small that finding them is not always so easy, the local stability of successful gaits can be evaluated by the return map as introduced in II-C.

The discrete state at the Poincaré section that is used

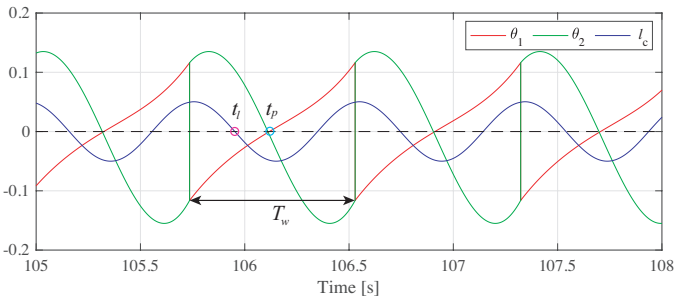

Fig. 11. Phase difference between walker and wobbling mass

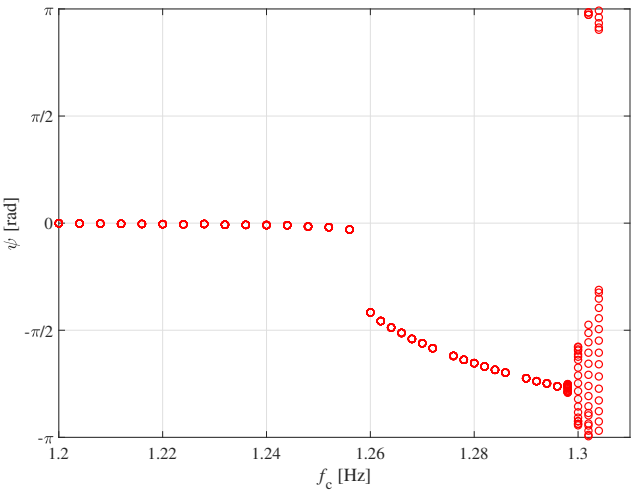

Fig. 12. Phase difference versus wobbling frequency

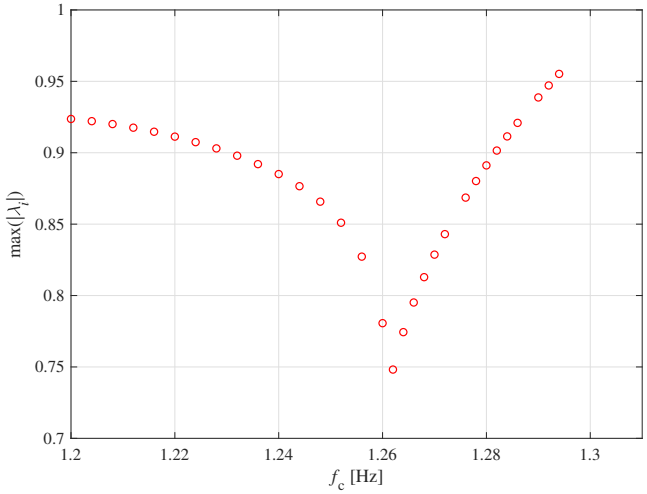

Fig. 13. Maximum absolute eigenvalue versus wobbling frequency.

for the return map is normally defined as the collection of the periodical points in the generalized coordinate and their time derivatives. Consequently, the state is defined as $\boldsymbol{Q} = \left[\theta_1^+ \ \theta_2^+ \ l_c^+ \ \dot{\theta}_1^+ \ \dot{\theta}_2^+ \ \dot{l}_c^+ \right]^{\mathrm{T}}$. However, the existence of time t in the controller u makes the system non-autonomous [22]. To simply convert the QPDW model to an autonomous system, we can augment the state vector with an extra element $\beta = \frac{2\pi t}{T_w}$ [16], [23]. Therefore, the state becomes:

$$\boldsymbol{Q} = \left[\theta_1^+ \ \theta_2^+ \ l_c^+ \ \dot{\theta}_1^+ \ \dot{\theta}_2^+ \ \dot{l}_c^+ \ \beta \right]^{\mathrm{T}}. \tag{20}$$

The maximum absolute eigenvalues are calculated using Eqs. (9) and (20). The results are plotted in Fig. 13. Here, only steady state gaits are utilized, since the evaluation of local stability of disordered gaits is meaningless. It is shown that all the steady state gaits (synchronized) in Fig. (7) are locally stable in the sense that the maximum absolute eigenvalues are less than 1 for all cases. This indicates that the steady state QPDW gait is capable of returning to itself after being slightly disturbed.

D. Effect of Forcing Amplitude

The simulation results in V-A show that the amplitude of hip angle can be efficiently excited by the periodical wobbling motion. It is therefore necessary to observe the effect of the forcing amplitude A_m.

The forcing amplitude is varied under two conditions: 1) $A_m = 0.2$ [m], and 2) $A_m = 0.02$ [m]. As shown in Fig. 14 (a), the entrained ranges are different for these two conditions. Fig. 14 (b) shows that there is also a jump in the impact hip angle under the condition of $A_m = 0.02$ [m] and so does the speed in Fig. 14 (c). On the other hand, no such jump occurs under the condition of $A_m = 0.2$ [m]. This phenomenon can be explained by the phase difference in Fig. 14 (d). According to Eqs. 18 and 19, anti-phase relationship implies efficient energy injection to the walker. In contrast to the speed, the efficiency of $A_m = 0.02$ [m] is much better than the condition of $A_m = 0.2$ [m] as shown in Fig. 14 (e). Moreover, local stabilities of the steady state gaits are guaranteed for both conditions as shown in Fig. 14 (f).

VI. CONCLUSION AND FUTURE WORK

Although the walker presented in this paper has only one actuator, it is capable of walking extremely efficiently on the level ground via our QPDW control method. The passive dynamics is positively utilized by initializing the gait from the fixed Poincaré section of PDWGD and exciting the hip angle indirectly and smoothly. The reason for inducing low speed walking is theoretically analyzed from the coupled oscillator and potential barrier point of view. Consequently, low speed walking can be avoided successfully.

Regarding the efficiency, walking gait with no energy cost using spring mechanism [24] has been already generated. Inspired by their work, one of the authors also have investigated non-powered gait with double-limb support phase [25] to provide further possibilities. Unlike these works, which do not require external actuation by appropriately avoiding ground collisions, our QPDW gait proposed in this paper injects kinetic energy into the walker. The periodical excitation of the wobbling motion, which injects kinetic energy, plays a similar role as the gravity induces passive dynamic walking. Compared to the non-powered gait, our QPDW gait is of course less efficient. It is however more robust when a slight perturbation, which is inevitable in the real-world, is added to the system. Moreover, we are taking step motion, that is, stance-leg exchange into account. Our future work will consider enlargement of the basin of attraction of the limit cycle to further enhance the stability [26]. Kinetic energy consumed by the ground collisions will be minimized according to the spring mechanism mentioned above. Moreover, experimental studies of a real machine according to Fig. 2 shall be also conducted and reported soon.

REFERENCES

[1] L. Amy, "Make robot motions natural," *Nature*, Vol. 565. pp. 422-424. 2019.

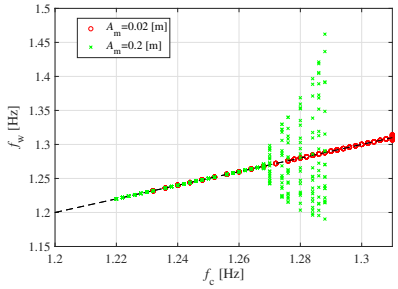

(a) Walking frequency versus wobbling frequency.

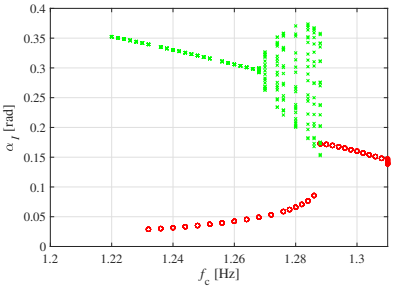

(b) Impact hip angle versus wobbling frequency.

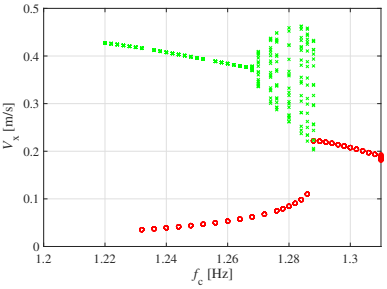

(c) Walking speed versus wobbling frequency.

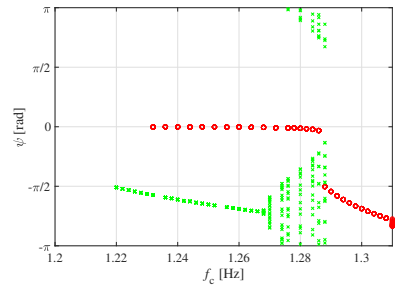

(d) Phase difference versus wobbling frequency.

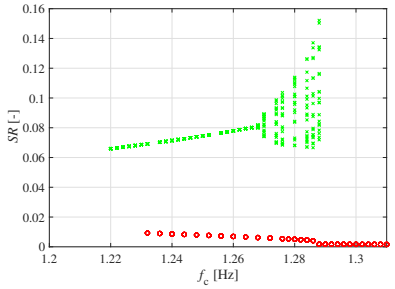

(e) Specific resistance versus wobbling frequency.

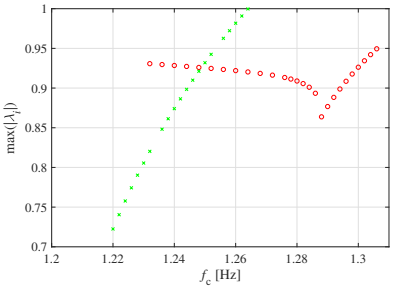

(f) Maximum absolute eigenvalue versus wobbling frequency.

Fig. 14. Effect of forcing amplitude.

[2] ATLAS, "Boston dynamics: Humanoid robot ATLAS," Available: https://www.bostondynamics.com/atlas/.

[3] M. Hutter, C. Gehring, D. Jud, et al, "Anymal-a highly mobile and dynamic quadrupedal robot," *Proceedings of the IEEE/RSJ International Conference on Intelligent Robots and Systems*, pp. 38-44, 2016.

[4] G. Bledt, M. J. Powell, B. Katz et al, "Mit cheetah 3: Design and control of a robust, dynamic quadruped robot," *Proceedings of the IEEE/RSJ International Conference on Intelligent Robots and Systems*, pp. 2245-2252, 2018.

[5] D. G. E. Hobbelen and M. Wisse, "Limit cycle walking", *Humanoid Robots, Human-like Machines*, IntechOpen, 2007.

[6] Y. Ikemata, A. Sano, H. Fujimoto, "A physical principle of gait generation and its stabilization derived from mechanism of fixed point," *Proceedings of the IEEE International Conference on Robotics and Automation*, pp. 836-841, 2006.

[7] T. McGeer, "Passive dynamic walking," *The International Journal of Robotics Research*, Vol. 9, No. 2, pp. 62–82, 1990.

[8] A. Goswami, B. Thuilot, and B. Espiau. "Compass-Like Biped Robot Part I: Stability and Bifurcation of Passive Gaits," *Res. Rep. INRIA*, 1996.

[9] S. H. Collins, M. Wisse, A. Ruina; R. Tedrake, "Efficient bipedal robots based on passive-dynamic Walkers," *Science*, Vol. 307, pp. 1082-1085, 2005.

[10] A. Goswami, B. Espiau and A. Keramane, "Limit cycles in a passive compass gait biped and passivity-mimicking control laws," *Autonomous Robots*, vol. 4, no. 3, pp. 273-286, 1997.

[11] M. W. Spong, 'Passivity-based control of the compass gait biped," *The IFAC 1999 World Congress*, pp. 19-23,1999.

[12] F. Asano, Z. Luo and M. Yamakita, "A novel gait generation for biped walking robots based on mechanical energy constraint," *IEEE Transactions on Robotics and Automation*, Vol. 20, No. 3, pp. 565-573, 2004.

[13] R. Tedrake, "Underactuated Robotics: Algorithms for Walking, Running, Swimming, Flying, and Manipulation ," *(Course Notes for MIT 6.832)*, Available: http://underactuated.mit.edu/

[14] S. Yasuhiro, and K. Osuka, "Walking control of quasi passive dynamic walking robot "Quartet III" based on continuous delayed feedback control," *Proceedings of the IEEE International Conference on Robotics and Biomimetics*, PP. 606-611, 2004.

[15] D. Tanaka, F. Asano and I. Tokuda, "Gait analysis and efficiency improvement of passive dynamic walking of combined rimless wheel with wobbling mass," *Proceedings of the IEEE/RSJ International Conference on Intelligent Robots and Systems*, pp. 151-156, 2012.

[16] F. Iida and R. Tedrake, "Minimalistic control of biped walking in rough terrain," *Autonomous Robots*, Vol. 28, No.3, pp. 355-368, 2010.

[17] F. Asano and I. Tokuda, "Indirectly controlled limit cycle walking of combined rimless wheel based on entrainment to active wobbling mass," *Multibody System Dynamics*, Vol. 34, Iss. 2, pp. 191-210, 2015.

[18] L. Li, I. Tokuda and F. Asano, "Optimal input waveform for an indirectly controlled limit cycle walker," *Proceedings of the IEEE/RSJ International Conference on Intelligent Robots and Systems*, pp. 7454-7459, 2018.

[19] L. Li, F. Asano and I. Tokuda, "Nonlinear analysis of an indirectly controlled sliding locomotion robot," *Proceedings of the IEEE/RSJ International Conference on Intelligent Robots and Systems*, pp. 8221-8226, 2018.

[20] L. Li, F. Asano, I. Tokuda, "High-speed sliding locomotion generation on slippery surface of an indirectly controlled robot with viscoelastic body," *IEEE Robotics and Automation Letters*, Vol. 4, Issue 3, pp. 2950-2957, 2019.

[21] F. Asano, I. Tokuda and Y. Akutsu, "Analysis of wobbling mass as shock-absorber in limit cycle walking and its application to micro vibration modeling," *Proceedings of the International Conference on Ubiquitous Robots and Ambient Intelligence*, pp. 224-229, 2014.

[22] T. S. Parker and L. O. Chua, "Practical Numerical Algorithms for Chaotic Systems," Springer-Verlag, 1989.

[23] P. Liljebäck, K. Y. Pettersen, Ø. Stavdahl, and J. T. Gravdahl, "Stability analysis of snake robot locomotion based on Poincaré maps," *Proceedings of the IEEE/RSJ International Conference Intelligent Robots and Systems*, pp. 3623-3630, 2009.

[24] G. Mario, and A. Ruina, "Walking model with no energy cost," *Physical Review E*, Vol. 83, No.3, pp.032901, 2011.

[25] F. Asano, "Non-powered stealth walking approach to generation of passive dynamic gait on horizontal plane," *Proceedings of the 12th IFAC Symposium on Robot Control*, pp.67-72, 2018.

[26] A. Engel, M. Bouten, A. Komoda, et al, "Enlarged basin of attraction in neural networks with persistent stimuli," *Physical Review A*, Vol. 42, No. 8, pp. 4998-5005, 1990.